Available online at www.sciencedirect.com

ScienceDirect

Journal of the European Ceramic Society 34 (2014) 2299–2309

www.elsevier.com/locate/jeurceramsoc

Large strains accompanying field-induced ergodic phase-polar ordered phase transformations in $Bi(Mg_{0.5}Ti_{0.5})O_3$–$PbTiO_3$–$(Bi_{0.5}Na_{0.5})TiO_3$ ternary system

Wanli Zhao, Ruzhong Zuo *, Jian Fu, Min Shi

Institute of Electro Ceramics & Devices, School of Materials Science and Engineering, Hefei University of Technology, Hefei 230009, PR China

Received 17 October 2013; received in revised form 3 January 2014; accepted 28 January 2014
Available online 24 February 2014

Abstract

A composition-induced pseudocubic–tetragonal structural transition was found to be accompanied by a relaxor phase transformation in $xBi(Mg_{0.5}Ti_{0.5})O_3$–$(0.75-x)PbTiO_3$–$0.25(Bi_{0.5}Na_{0.5})TiO_3$ ternary solid solutions. Dielectric and ferroelectric measurements suggest the coexistence of ergodic and nonergodic relaxor phases within a single pseudocubic phase zone for samples with $0.50 < x < 0.51$ where large electromechanical strains of up to 0.43% (S_{max}/E_{max} = 621 pm/V) can be generated. The mechanism was mainly ascribed to the accumulated effects of field-modulated continuous and reversible transformations from a pseudocubic ergodic phase to a rhombohedral short-range ordered phase (but not nonergodic polar phase), and finally to a long-range ordered ferroelectric tetragonal phase. These procedures were found to be strongly dependent on the applied field magnitudes. These findings were reasonably approved by a couple of measurements such as dielectric–temperature–frequency spectrum, ferroelectric polarization/strain hysteresis loops, polarization current density curves and particularly ex situ Raman spectrum and in situ high-resolution synchrotron X-ray diffraction.

Keywords: Perovskite; Relaxor; Giant strain; Phase transition

1. Introduction

Structural transformations accompanying large electrostrains have found wide applications in actuators in the last decades. Of many types of these materials with such performances, $PbZrO_3$ (PZ)-based antiferroelectric materials have been considered as the most outstanding candidate since a large strain (volume effect) could be generated during an electric field induced antiferroelectric–ferroelectric phase transition.[1–4] Their strain levels (up to 0.85%)[3,4] are much larger than those observed in typical relaxor ceramics (for example, $Pb(Mg_{1/3}Nb_{2/3})O_3$) with an electrostrictive effect,[5–7] and even in typical ferroelectric ceramics with a strong piezoelectric response.[8,9] That is to say, the intrinsic contribution from the phase transformation usually plays an important role in the evolution of large strains, compared to the extrinsic contribution such as domain switching since a high strain value is rather difficult to achieve in polycrystalline ceramics owing to the clamping effect from neighboring domains and grains with different orientations.[10]

In recent years, giant strains of ~0.4% have been realized in bismuth-containing perovskite compounds under a high bias field.[11–15] The $(Bi_{0.5}Na_{0.5})TiO_3$–$BaTiO_3$ (BNT-BT)-based systems were initially found to own such a giant electrostrain.[11–13] These compositions basically include donor doped BNT-BT/KBT,[12,14] and BNT-BT based solid solutions.[11,13,15] The evolution of large strains in BNT-based compositions seems to always correlate with the down-shift of high-temperature relaxor phase zone after the compositional modification. It was considered in the early period as a consequence of the field induced antiferroelectric to ferroelectric phase transformation resembling the above-mentioned PZ-based ceramics, generally because of pinched polarization versus electric field (*P*–*E*) hysteresis loops.[11] Although this process was detected particularly by an acoustic emission measurement,[16] the indication of antiferroelectric phase zone still lacks strict experimental evidences. The transition of nonpolar phase into polar phase was

* Corresponding author. Tel.: +86 551 62905285; fax: +86 551 62905285.
E-mail addresses: rzzuo@hotmail.com, piezolab@hfut.edu.cn (R. Zuo).

0955-2219/$ – see front matter © 2014 Elsevier Ltd. All rights reserved.
http://dx.doi.org/10.1016/j.jeurceramsoc.2014.01.040

later on suggested to explain how the large strain can be produced in these compositions.[13] The judgment of such a nonpolar phase denoting the high-temperature relaxor phase zone in BNT-based system generally depends on the frequency-dependent and diffuse dielectric behavior, although some recent investigations reported the structural evidence of the relaxor phase as well as the temperature-dependent macroscopic data.[17–20] This question is still open for discussion and the mechanism for such a large electrostrain seems to need more direct and stronger experimental supports.

Apart from BNT-based compositions, $Bi(Mg_{0.5}Ti_{0.5})O_3$–$PbTiO_3$ (BMT-PT) binary systems were also reported to have similar large-strain electromechanical behavior through adding a few amount of second phases such as $BaZrO_3$, $PbZrO_3$ and so on.[21,22] These second phases were considered to play a crucial role in down-shifting the antiferroelectric phase zone possibly existing at a higher temperature range in pure BMT whose structure was believed to resemble the typical PZ.[23] Because of this, the origin of large electrostrains in BMT-PT based ternary systems was also ascribed by J Chen et al., to a field-forced phase transition from antiferroelectric to ferroelectric phases.[21,22] Similarly, pinched *P–E* loops were used as an indirect proof of the existence of antiferroelectric phases. If compared, it is interesting to note that maximum electrostrains of the same level (~0.40–0.43%) under 6–7 kV/mm were generated in BNT-based and BMT-based compositions, which are comparable to those of soft PZTs,[24,25] but obviously smaller than those from the unit cell volume change in an antiferroelectric material.[3,4] This would suggest that the large-strain-generating mechanism for Bi-containing materials (BNT based and BMT-based, etc.,) should have something in common, but seems to be different from that for PZ-based antiferroelectrics. Another strategy to achieving a large electrostrain in PZ substituted BMT-PT was studied recently by maintaining a fixed content of PT to keep all compositions lying at a pure rhombohedral phase side.[26] Surprisingly, equivalent strain levels (0.39%) for an excitation field of 6 kV/mm were produced although no phase structural transition was involved and only the relaxor degree changes with composition. Moreover, large electrostrains were also reported to appear in other systems such as $CaZrO_3$-modified alkaline niobates whose individual grains were chemically modulated to have a duplex structure composed of a polar core and nonpolar shell.[27] The nonpolar shells were considered to play a significant role in the high strain effect in terms of efficient polarization extension from the cores and its easy release.[28] The coexistence of nonpolar and polar phases was also sometimes believed to occur in BNT-based systems,[13] resulting in a large strain during the nonpolar–polar phase transition. Therefore, the combination of all these results in the literature would bring us to ponder over what really happens in these Bi-containing systems after an external field is applied.

In this work, a new composition system of xBMT–$(0.75-x)$PT–0.25BNT was constructed by putting two systems BNT and BMT-PT together in terms of their respective phase transition behavior and fascinating strain characteristics. The aim to do so is to see how the new system behaves, whether the strain effect can be adjusted or not and particularly to explore what really contributes to such a large electrostrain. The selected composition points were drawn in a phase diagram as shown in Fig. 1, being distributed on both sides of an approximate morphotropic phase boundary (MPB) line of BNT-PT and BMT-PT binary systems by fixing a constant BNT content of 25%. The substitution of BMT for PT was found to not only induce a morphotropic phase structural transformation from pseudocubic (PC) to tetragonal (T) ferroelectric phases, but also generate a giant electrostrain (~0.43%) excited by a high external field within a pure pseudocubic phase zone. Ex situ Raman spectra and in situ synchrotron X-ray diffraction were applied to explore the change of local micro-structures and macro phase structures upon the application of electric fields of different magnitudes. Together with the composition–temperature–structure phase diagram, ferroelectric polarization/strain hysteresis loops and polarization current density curves, the mechanism for generating large electrostrains was specially discussed.

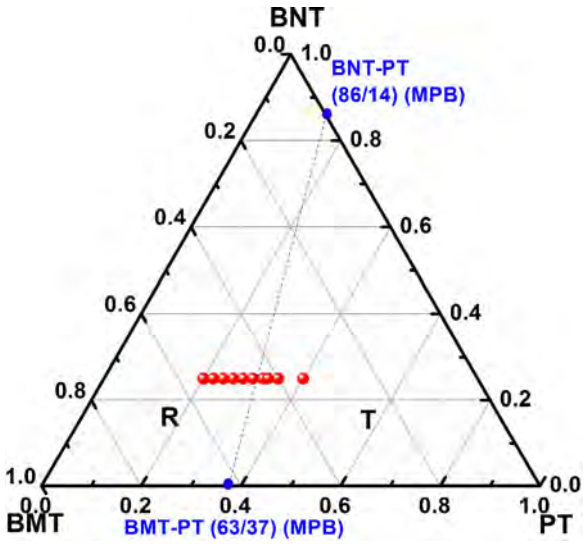

Fig. 1. Schematic phase diagram of BMT-PT-BNT ternary system.

2. Experimental

The xBi$(Mg_{0.5}Ti_{0.5})O_3$–$(0.75-x)PbTiO_3$–$0.25(Bi_{0.5}Na_{0.5})TiO_3$ (xBMT-PT-BNT, $x = 0.35$–0.55) ceramics were synthesized by a conventional solid-state reaction method using high-purity Bi_2O_3, TiO_2, Na_2CO_3, PbO and $(MgCO_3)_4{\cdot}Mg(OH)_2{\cdot}5H_2O$ as raw-materials. After weighing according to the stoichiometric formula, the powders were ball-milled with ethanol and zirconia media for 6 h. The dried powders were calcined twice at 850 °C for 2 h and then ball milled again for 8 h. The powders were uniaxially pressed into pellets with 10 mm in diameter and the pellets were sintered in sealed crucibles at 1080–1100 °C for 2 h. For electrical measurements, the silver paste was painted on major sides of the samples and fired at 550 °C for 30 min. The samples were poled under a dc field of 4 kV/mm at 120 °C for 15 min in silicone oil.

The relative densities were evaluated by the Archimedes method. A relative density of >97% can be achieved for all the studied samples. The crystal structure was examined by an X-ray diffractometer (XRD, D/Max-RB, Rigaku, Japan) in the 2θ range of 20–60°. The microstructure was observed using a scanning electron microscope (SEM, JEOL JSM-6490LV, Tokyo, Japan). Before the SEM observation, the fractured surface was polished and etched by heat treatment at 980 °C for 30 min. Dielectric properties were measured as a function of temperature and frequency by an LCR meter (Agilent E4980A, Santa Clara, CA). *P–E* hysteresis loops and electric field-induced strain (*S–E*) curves were measured as a function of composition and temperature under bipolar and unipolar fields using a ferroelectric measuring system (Precision multiferroelectric, Radiant Technologies Inc., Albuquerque, NM) connected with an accessory laser interferometer vibrometer (AE SP-S 120E, SIOS Meβtechnils, GmbH, llmenau, Germany). The piezoelectric constant d_{33} was measured by a Belincourt-meter (YE2730A, Sinocera, Yangzhou, China). Ex situ Raman spectrum (633 nm, LabRAM HR800, HJY, Longjumeau Cedex, France) was obtained on samples after being poled under different electric fields at room temperature. The spectral parameters such as wavenumber and full width at half maximum (FWHM) were extracted by deconvoluting the spectra according to multiple Gaussian–Lorentzian peak functions. For in situ synchrotron X-ray diffraction measurement, thin gold electrodes were sputtered onto two well-polished sides of the ceramic disks with ~8 mm in diameter and ~40 μm in thickness. High resolution X-ray diffraction was taken at Shanghai Synchrotron Radiation Facility (SSRF) using beam line 14B1 (λ = 1.2378 Å). The beam size at the sample position is about 0.3 mm × 0.3 mm. The grain size of the samples for the synchrotron radiation is about 1–4 μm. Therefore, the collected diffraction data would disclose the statistical average structure information.

3. Results

3.1. Composition-dependent phase structural transformation and microstructure

Fig. 2 shows the phase structural change of *x*BMT-PT-BNT solid solution ceramics with the substitution of BMT for PT. It is obvious that all studied compositions demonstrated a single perovskite structure in terms of typical diffraction patterns (Fig. 2(a)). Moreover, it can be seen that a typical tetragonal symmetry could be identified as $x \leq 0.47$, as evidenced by the peak splitting of the (0 0 2) and (2 0 0) diffraction lines. With increasing the BMT content ($x \geq 0.50$), the (0 0 2) and (2 0 0) peaks merged gradually into a single one, indicating that the *x*BMT-PT-BNT solid solutions undergo a transition from a single tetragonal phase to a pure rhombohedral or pseudocubic phase. Furthermore, a careful observation of the (1 1 1) peak indicated no obvious peak splitting, such that the possibility of a rhombohedral phase could be excluded. This conclusion could be further confirmed by a high-resolution X-ray diffraction analysis as discussed later. Detailed XRD scans (Fig. 2(b)) for all samples in a 2θ range from 43° to 48° have clearly indicated

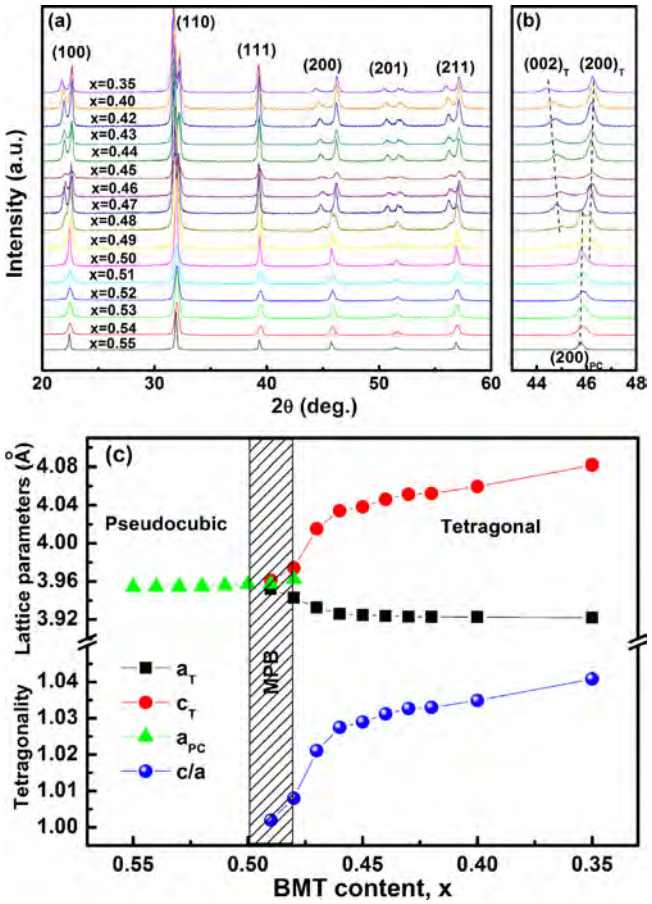

Fig. 2. (a) Room-temperature XRD full patterns, (b) the (2 0 0) diffraction lines and (c) the calculated lattice parameters of *x*BMT-PT-BNT ceramics as a function of the BMT content.

the suggested phase transition behavior while the MPB between tetragonal and pseudocubic phases could be identified roughly in the composition range of $0.47 < x < 0.50$. The structural parameters, which were calculated by fitting the diffraction peak profile with a pseudo-Voigt profile function using the program of MDI Jade, are shown in Fig. 2(c). In the pseudocubic phase zone, it can be seen that the lattice constant a_{PC} exhibited a little increase with decreasing the BMT content x. By comparison, the lattice constant c_T in the tetragonal phase zone increased rapidly, however the lattice constant a_T decreased slowly with decreasing the BMT content. As a result, the tetragonality (c/a) increased with decreasing the BMT content, which is believed to be a result of the increasing coupling between *A*-site Pb/Bi cations and *B*-site ferroelectrically active cations such as Ti^{4+} and Mg^{2+}. On the one hand, ferroelectrically active ions can form short, covalent bonds with oxygen in the form of BO_6 octahedra. Because Mg^{2+} has a weaker electronegativity than Ti^{4+}, the angle of the BO_6 tilts would be increased with decreasing the BMT content. On the other hand, as the electronegativity of Bi^{3+} is weaker than that of Pb^{2+}, the substitution of Pb^{2+} for Bi^{3+} can enhance the *A–B* atomic displacement coupling, resulting in an increase of the *B*-site displacement.

In addition to the variation of phase structures, the microstructure of the sintered samples may also be composition dependent

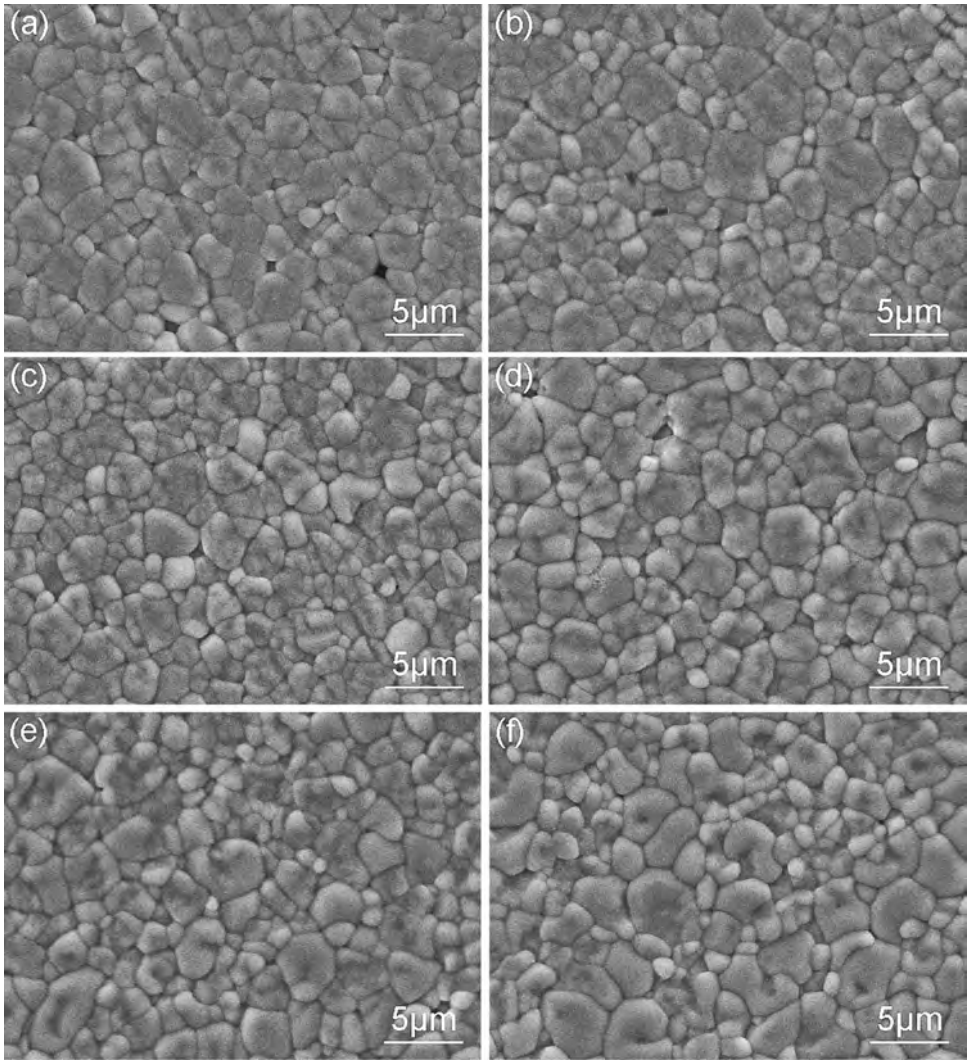

Fig. 3. SEM micrographs of *x*BMT-PT-BNT ceramics sintered at 1080 °C: (a) $x = 0.55$, (b) $x = 0.53$, (c) $x = 0.51$, (d) $x = 0.49$, (e) $x = 0.47$, (f) $x = 0.40$.

to a certain degree. Fig. 3 shows the SEM micrographs of the polished and etched *x*BMT-PT-BNT ceramics sintered at 1080 °C. The results indicate that all the samples have high densities and well-developed grains. Moreover, it can be seen that the change of the BMT content has only a slight effect on the grain size and morphology of *x*BMT-PT-BNT ceramics. The average grain size of different samples seems to be in the range of 1–4 μm.

3.2. Spontaneous relaxor to ferroelectric phase transition and ergodic to nonergodic phase transition

The dielectric properties of unpoled *x*BMT-PT-BNT ceramics were plotted as a function of temperature and frequency, as shown in Fig. 4. It can be seen from Fig. 4(a) that the temperature at the dielectric maxima (T_m) increased with decreasing the BMT content x. It increased from 308 °C at $x = 0.55$ to 346 °C at $x = 0.45$. The increase of the ferroelectric phase transition temperature is usually ascribed to the enhancement of the tetragonality for a couple of perovskite solid solution ceramics (see Fig. 2).[29] Meanwhile, the dielectric constant values ε_m at T_m at a fixed frequency of 1 kHz rapidly decreased with increasing the BMT content in addition to the increased diffuseness of dielectric peaks. The maximum ε_m values did not appear in the composition near MPB. This phenomenon was also observed in some other MPB composition systems, such as in $PbTiO_3$–$BiScO_3$ system where it was explained in terms of the connectivity between the TiO_6 octahedron and ScO_6 octahedron in the perovskite structure.[30]

Moreover, a typical relaxor phase transition behavior around T_m was clearly observed for samples with higher BMT contents such as $x = 0.55$ and $x = 0.51$ (Fig. 4(b)), which are characterized by the diffuse phase transition (DPT) and the frequency dispersion of the dielectric constant. This feature is obviously different from that of BMT-PT or BNT-PT binary system, which usually only exhibits a diffuse phase transition behavior at the dielectric maxima.[31,32] As an example, the deviation degree ($\Delta T_m = 254$ °C) from the Curie–Weiss law[33] for the 0.55BMT-PT-BNT sample measured at 100 kHz is indicated as a lower inset of Fig. 4(b). It was calculated by using the equation $\Delta T_m = T_{cw} - T_m$ where T_{cw} denotes the temperature

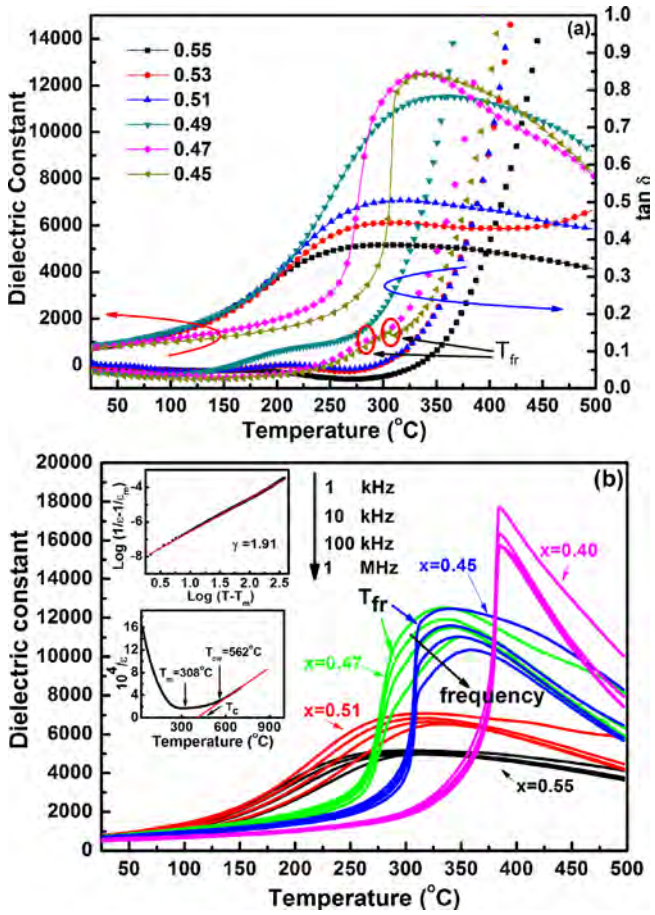

Fig. 4. (a) Dielectric constant and dielectric loss at 1 kHz as a function of temperature for unpoled *x*MBT-PT-BNT samples, and (b) frequency-dependent dielectric constants versus temperature curves of unpoled samples. The insets show the deviation from the Curie–Weiss law (lower one) and the diffuseness degree (upper one) of the $x = 0.55$ sample, respectively.

from which the dielectric permittivity starts to deviate from the Curie–Weiss law. Furthermore, the diffuseness degree (γ) of the same composition calculated from a modified Curie–Weiss law[34] was determined to be 1.91 from the slope of the fitted lines, as shown in the upper inset of Fig. 4(b). Large values of γ and ΔT_m revealed that the $x = 0.55$ sample exhibits a nearly complete DPT. In addition, the parameter ΔT_{relax}, which is defined as the difference between two T_m values measured at 1 MHz and 1 kHz, was introduced to investigate the relaxation degree of ferroelectric ceramics.[33,35] It was calculated to be about 45 °C for the $x = 0.55$ sample, indicating a significant frequency dispersion. Both ΔT_m (or γ) and ΔT_{relax} tend to increase with increasing the BMT content for *x*BMT-PT-BNT samples with $x = 0.35$–0.55. That is to say, the substitution of BMT for PT would tend to disrupt the ferroelectric long-range ordered state, making it exist at a lower temperature range. As a result, stronger and stronger relaxor behavior was induced in this new ternary system. Most interestingly, a spontaneous ferroelectric to relaxor phase transition temperature T_{fr} started to be observed from the $x = 0.47$–0.48 samples which exhibit a normal dielectric behavior near room temperature but a typical dielectric relaxor behavior at higher temperatures, as clearly indicated in loss tangent versus temperature curves (Fig. 4(a)). Therefore, a pseudocubic to tetragonal crystal structural transformation at room temperature was just accompanied by a relaxor to ferroelectric phase transition owing to the substitution of BMT for PT.

It was generally believed that relaxor systems are characterized by local polar nanometer-sized regions (PNRs) that usually appear at temperatures a few hundred degrees above the Curie temperature,[36–39] where the macroscopic polarization completely disappears. At this temperature range, the PNRs are randomly distributed and exist in an ergodic state. Moreover, the size and dynamics of PNRs were believed to play an important role in the relaxor behavior.[37,40,41] Upon cooling, the average size of PNRs increases and their dynamics slows down enormously, such that at an extremely low temperature the PNRs in an ergodic relaxor either become sufficiently large to transform into micron-sized domains, i.e., the formation of normal ferroelectrics below T_{fr},[40,42] or simply freeze into a static polar order at temperatures below a critical freezing temperature T_f, i.e., the nonergodic relaxor.[40,43] Therefore, it can be believed that the samples should exhibit an ergodic relaxor state or a nonergodic relaxor state with an average pseudocubic symmetry (see Figs. 2 and 4) at room temperature in the composition range of $x = 0.50$–0.55, but a normal tetragonal ferroelectric ordered state at room temperature in the range of $x < 0.47$. In the composition range of $0.47 < x < 0.50$ (MPB), the samples should be a mixture of pseudocubic relaxor ferroelectric state and tetragonal normal ferroelectric state. In addition, as can be seen in Fig. 4(a), the rapid decrease of the ε_m value with increasing the BMT content could also confirm the disruption of the ferroelectric long-range order and the appearance of the PNRs in *x*BMT-PT-BNT system. As the compositions entered into the relaxor phase zone, the decrease of the domain size was accompanied by the formation of PNRs. The coupling between these PNRs became weaker, resulting in a decrease of the ε_m value. Similar phenomena have been observed in other systems.[12,21,27]

In order to further elucidate the exact phase structure of *x*BMT-PT-BNT ceramics, temperature-dependent *P*–*E* hysteresis loops and bipolar strain curves of the chosen *x*BMT-PT-BNT ceramics were measured, as shown in Fig. 5. Meanwhile, the corresponding polarization current densities versus electric field (*J*–*E*) curves were also recorded. With increasing the BMT content, the PNRs would become more active and smaller, such that they could more easily switch back to a disordered state when the applied electric field was removed. Therefore, the $x = 0.53$ sample showed a slim *P*–*E* loop with very small remanent polarization and a low-hysteresis *S*–*E* loop with a nearly zero negative strain (Fig. 5(a) and (b)), typical of an ergodic relaxor phase. The bipolar strains exhibited similar loops and zero negative strains in the whole measuring temperature range for the $x = 0.53$ sample (see Fig. 5(b)), indicating that the ergodic relaxor state can be maintained in the whole measuring temperature range. By comparison, the samples with $x = 0.47$ and 0.49 were typical of the ferroelectric polar phase with features of macro-domain switching, as can be seen from the obvious square hysteresis loops and negative strains. With increasing temperature, the remanent polarization and negative strain values did not obviously change, indicating that the $x \leq 0.49$ compositions have entered into a

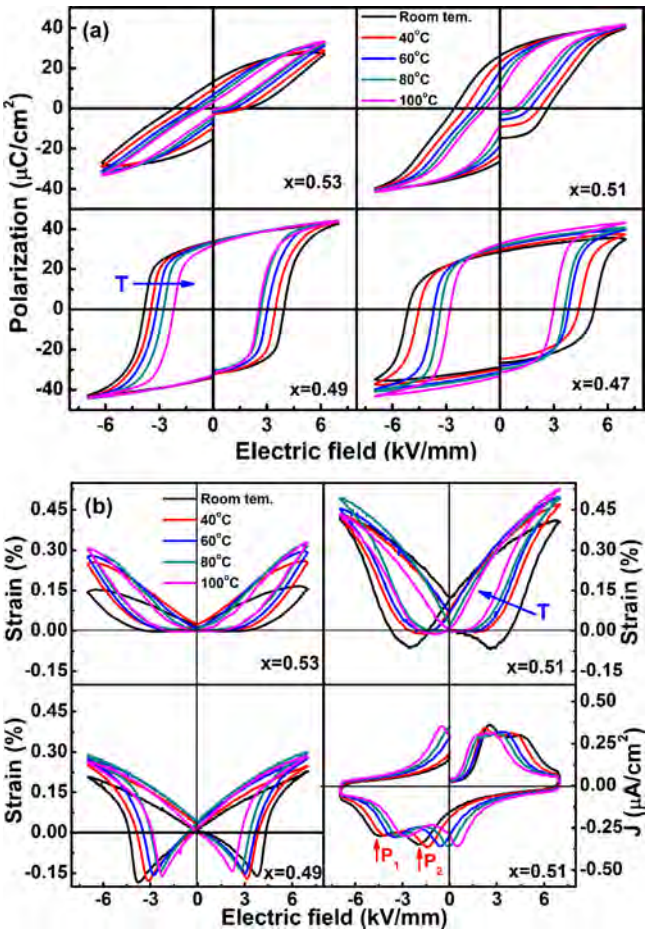

Fig. 5. (a) Temperature dependence of *P–E* hysteresis loops for *x*BMT-PT-BNT ceramics and (b) temperature dependence of bipolar *S–E* loops for *x*BMT-PT-BNT ceramics as well as the corresponding *J–E* curves for the $x = 0.51$ sample.

normal ferroelectric phase zone and no ergodic phases could appear in the measuring temperature range. Compared with the $x = 0.53$ and $x \leq 0.49$ samples, it is worthy of note that the $x = 0.51$ sample behaved a little differently in terms of its pinched *P–E* loops and small negative strain. In addition, as can be seen in Fig. 5(b), the negative strain of the $x = 0.51$ sample disappeared rapidly with increasing temperature up to 40 °C, which is only slightly higher than room temperature. These results indicated that this composition should be just located at the boundary of ergodic and nonergodic phases. This can be further confirmed if one compares the temperature dependent dielectric constant and loss tangent for different samples before and after poling, as shown in Fig. 6, because the ergodic phase could evolve reversibly into a long-range polar ferroelectric phase, while a nonergodic phase can irreversibly change into a long-range polar ferroelectric phase under the application of an electric field.[43] Accordingly, the $x = 0.49$ sample can be classified as a nonergodic relaxor owing to the presence of a T_{fr} point after poling. In contrast, the $x = 0.53$ sample can be recognized as an ergodic relaxor at room temperature because there is no T_{fr} point above room temperature for both unpoled and poled samples. By comparison, the $x = 0.51$ sample looks similar to the $x = 0.53$ sample, as can be seen from Fig. 6(c and d). However, it is found that the poling treatment has depressed the dielectric constant (Fig. 6(g)) and induced a small loss tangent peak (Fig. 6(h)), suggesting that there was indeed an irreversible phase transition process after poling. It can be thus inferred that this transition should correspond to an irreversible transition from a nonergodic relaxor to a long-range ordered ferroelectric. Moreover, as can be seen from the *J–E* curves (Fig. 5(b)) of the $x = 0.51$ sample, two obvious polarization current peaks could be observed while both of which shifted to lower field values with increasing the measuring temperature. This means that two kinds of phase transition processes might participate in the polarization switching. The meaning of the two current peaks will be discussed later.

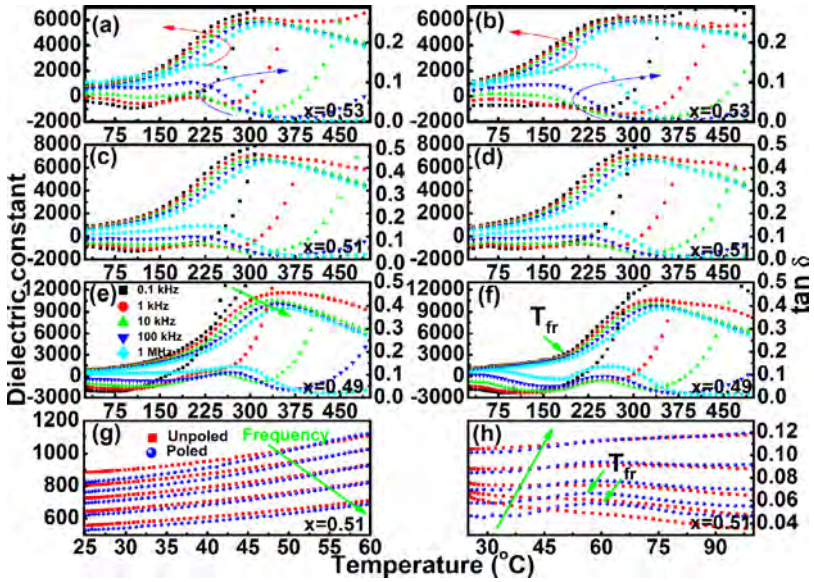

Fig. 6. The dielectric constant and loss tangent of unpoled (a, c and e) and poled (b, d and f) samples as a function of temperature and frequency. The comparison of the dielectric constant (g) and loss (h) at different frequencies of unpoled and poled ceramics with $x = 0.51$.

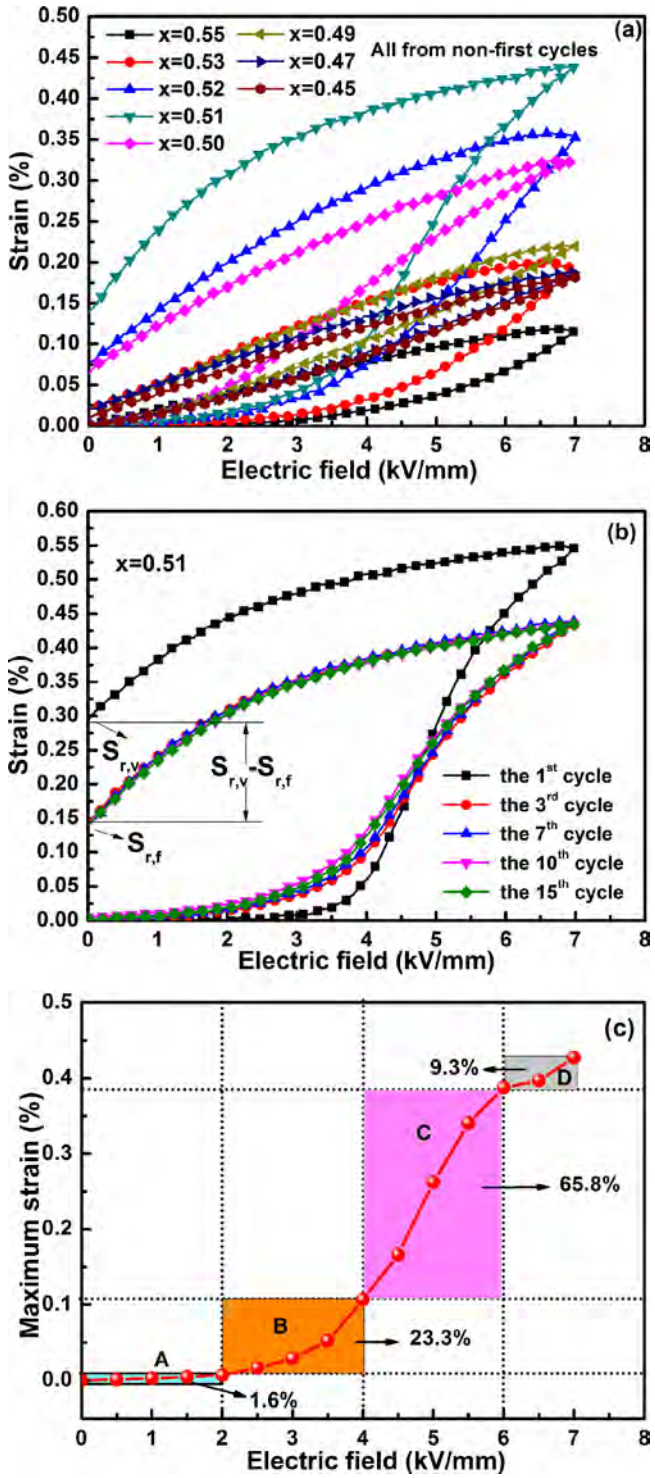

Fig. 7. (a) Unipolar *S–E* loops at 1 Hz on previously cycled *x*BMT-PT-BNT ceramics as a function of the BMT content, (b) unipolar *S–E* loops at 1 Hz of the $x = 0.51$ sample after different electric cycles and (c) the maximum strains as a function of the magnitude of the applied electric fields obtained from non-first cycles.

3.3. Large electrostrains of *x*BMT-PT-BNT ternary system

Fig. 7(a) displays unipolar electric field induced strain curves on previously cycled *x*BMT-PT-BNT ceramics at room temperature. With decreasing the BMT content *x*, the unipolar strains first increased significantly, and then reached a maximum value at $x = 0.51$ and finally started to decrease. A giant electrostrain of 0.43% at 7 kV/mm was surprisingly observed in the $x = 0.51$ sample. Moreover, one may find that most of the samples seemed to exhibit an obvious remanent strain (S_r) in the unipolar loops. That is to say, the unipolar loops are not closed. It is about 0.14% for the $x = 0.51$ sample under the current measuring condition, which might make one doubt whether this large electrostrain can be repeated or not, and whether the produced giant strain is useful or not. In order to clarify these issues, the unipolar strain loops from the 1st cycle on a virgin sample and from the 3rd, 7th, 10th and 15th cycles on a previously cycled sample are shown in Fig. 7(b). It can be obviously seen that the first-cycle strain loop showed a much larger S_r value (~0.3%) than that (~0.14%) for the non-first cycles. The difference of the remanent strains between the first cycle and the other cycles should be attributed to the really occurred irreversible process during electric cycling, which in this case can be referred to as the field forced nonergodic relaxor to ferroelectric phase transition and even non-180° ferroelectric domain switching (as the external driving field is high enough). Also, the above strain difference was found to be approximately equal to the difference of the maximum strains from the first cycle and non-first cycles. Therefore, the remanent strain value in the unipolar strain loops from non-first cycles should be false and was defined as $S_{r,f}$ infra. By comparison, the remanent strain value from the first cycle on a virgin sample was referred to as $S_{r,v}$. The origin of $S_{r,f}$ was believed to be associated with the hysteresis effect of the reversible ergodic relaxor to ferroelectric phase transition, which makes the ferroelectric testing system arbitrarily record a strain during electric field unloading to zero. This can be proved by the fact that all non-first unipolar strain loops were perfectly repeated, indicating that such a remanent strain ($S_{r,f}$) could disappear very shortly after removal of the applied field. It should be noted that the measurement between each cycle was done discontinuously with an interval of few seconds, So, the decay in the remanent strain ($S_{r,f}$) should be a time-dependent effect. Further, one may expect that if this is the case, the measurement at different signal frequencies should make a difference and even erase the above-mentioned $S_{r,f}$. Unfortunately, within the experimentally allowed measuring frequency range, the hysteresis behavior of the field induced ergodic relaxor to ferroelectric phase transition for the studied material system was not largely influenced, such that the strain measurement at different frequencies was not successful in removing the $S_{r,f}$ value. It has been reported that the electric field induced ferroelectric phase transition from ergodic phases at higher temperatures exhibit much weaker frequency dispersion than from nonergodic phases at lower temperatures.[44] According to the above analysis, the calculation of the normalized strains $d^*_{33} = S_{max}/E_{max}$ should be appropriate although the strain loops from non-first cycles were not closed (Fig. 7(a)).

The maximum strains generated under each electric field from non-first cycles were plotted as a function of the magnitude of applied fields, as shown in Fig. 7(c). A relatively small strain under low electric fields ($E < 2$ kV/mm, part A) was observed, which may correspond to a low field piezoelectric effect (maybe

partially from the electrostriction effect), taking up only ~1.6% of the total strain values. During this period, the reorientation and growth of the PNRs would occur as an electric field was applied. As the electric field was increased above 2 kV/mm, the strain curve did not obey the linear tendency any more, but underwent an *S*-shaped change with an inflection point at $E = 4$ kV/mm (part B for $E = 2$–4 kV/mm and part C for $E = 4$–6 kV/mm). A contribution of ~23.3% at Part B probably originated from some changes related to the ergodic phase in the sample, corresponding to the first polarization current peak P_1 (Fig. 5(b)). As the field was increased above 4 kV/mm, ~65.8% of the total strain from the part C was observed with a large strain hysteresis (see Fig. 7(a)), indicating that the domain switching might be one of the important mechanisms. At the same time, it means that the sample should belong to a complete polar ferroelectric state with a macroscopic domain structure as the field is larger than 4 kV/mm. Generally, the field induced domain switching would not make such a large contribution to the strain (~0.28% of 0.43%). Therefore, some other changes should be involved at the same time during this electric field range, inducing the second polarization current peak P_2 (Fig. 5(b)). As the electric field was increased from 6 kV/mm to 7 kV/mm, the remaining ~9.3% strains (part D) might be due to the further switching of ferroelectric domains. In a word, a series of changes might accompany the generation of large strains under the application of a high bias field.

3.4. Phase diagram of xBMT-PT-BNT ternary system

The room-temperature normalized strains d^*_{33} (S_{max}/E_{max}) and quasi-static piezoelectric coefficient d_{33} of *x*BMT-PT-BNT ceramics were plotted as a function of the BMT content *x*, as shown in Fig. 8(a). It can be seen that four phase zones (I, II, III and IV) could be separated in the whole composition range. The maximum d^*_{33} (621 pm/V, at $x = 0.51$) and d_{33} (205 pC/N, at $x = 0.49$) values were obtained in Zone II and Zone III, respectively. The best piezoelectric properties in Zone III (MPB) can be easily understood by the fact that the coexistence of pseudocubic and tetragonal phases (FE_T) provides more polarization vectors, making the polarization switching easier along the applied field direction.[10,45] Zone II denotes the coexistence zone of the ergodic phase and nonergodic phase at room temperature, which can transform into a complete ergodic phase above a critical freezing temperature T_f as determined by fitting the measured dielectric permittivity versus temperature curves (Fig. 4(b)) to the *Vogel–Fulcher* relationship.[46] The compositions in Zone I can be identified as a complete ergodic relaxor state at room temperature, for which a near zero quasi-static d_{33} was obtained. Zone IV corresponds to a typical ferroelectric phase with a tetragonal symmetry as identified by the X-ray diffraction analysis, dielectric and ferroelectric measurements. In summary, the composition–temperature phase diagram could be plotted, as shown in Fig. 8(b). It can be clearly seen that the samples at $T < T_{fr}$ belong to classical ferroelectric phases. The area marked by grids corresponds to the coexistence zone of ergodic and nonergodic phases in a certain composition/temperature range.

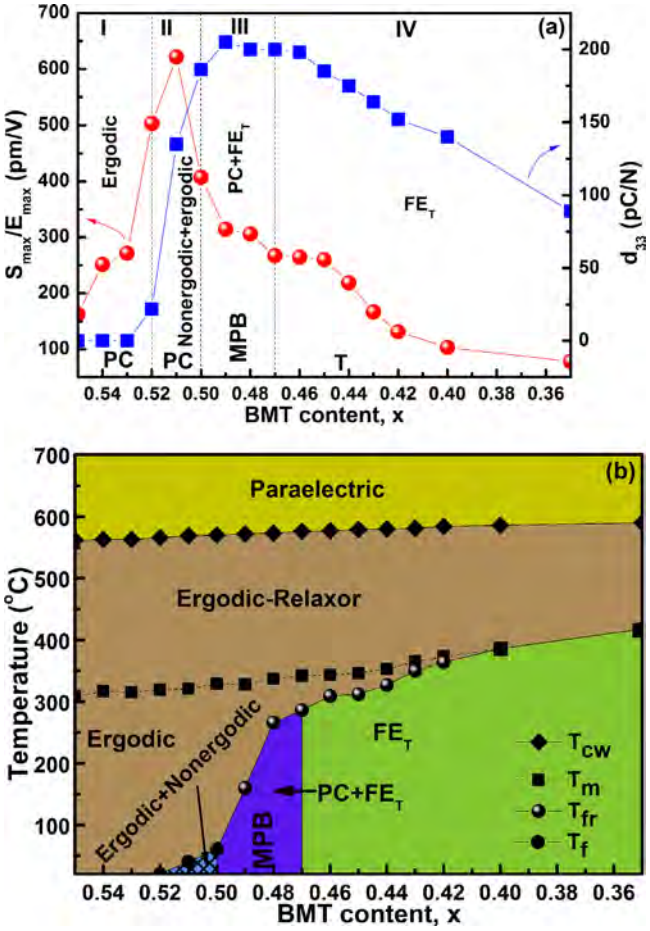

Fig. 8. (a) Normalized strain S_{max}/E_{max} (d^*_{33}) and quasi-static d_{33} as a function of the BMT content separated by four zones and (b) phase diagram of *x*BMT-PT-BNT ceramics. T_{cw}: the temperature from which the dielectric permittivity starts to deviate from the Curie–Weiss law; T_m: the dielectric maximum temperature; T_{fr}: the ferroelectric to relaxor phase transition temperature; T_f: the freezing temperature of ergodic PNRs.

4. Discussion

The electric field induced strains are generally correlated with the structural variation that happens in the sample driven by a high bias field. Fig. 9 shows *P–E* hysteresis loops and corresponding *J–E* curves at room temperature for various samples at a frequency of 1 Hz. With decreasing the BMT content, an obvious increase of the maximum polarization was observed as well as an evident change of the *J–E* curve, indicating the presence of different domain states. For the $x = 0.51$ and 0.50 samples, their *J–E* curves exhibited two obvious broad current peaks (P_1 and P_2), being centralized at ~2.7 kV/mm and ~4.8 kV/mm, respectively. These two electric field values are roughly located in the middle of part B and part C as shown in Fig. 7(c). As $x < 0.5$, only a single current peak could be observed which shifted toward the direction of higher electric fields because of the increased tetragonality. In order to clarify the evolution details related to the local structure and average crystal structure in response to the action of external fields, ex situ Raman spectra and in situ synchrotron X-ray diffraction measurement were specially measured on the $x = 0.51$ sample.

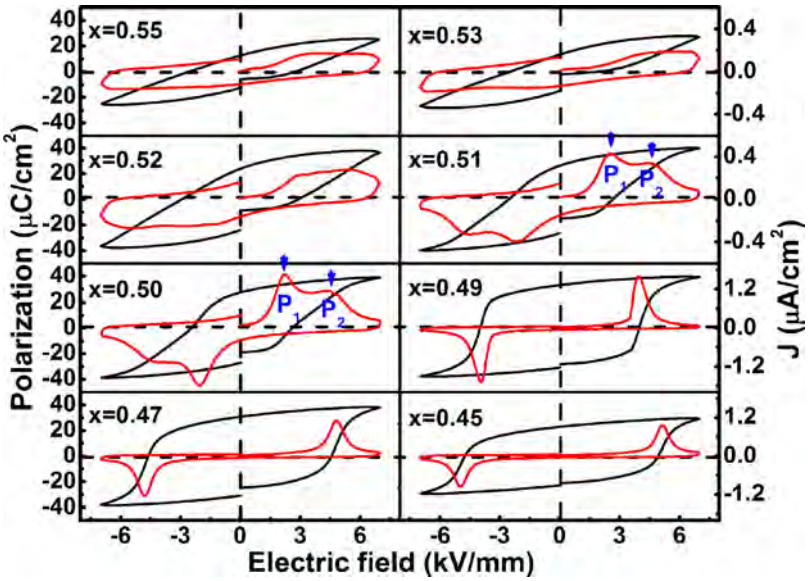

Fig. 9. *P–E* hysteresis loops and associated *J–E* curves of *x*BMT-PT-BNT ceramics measured at a frequency of 1 Hz.

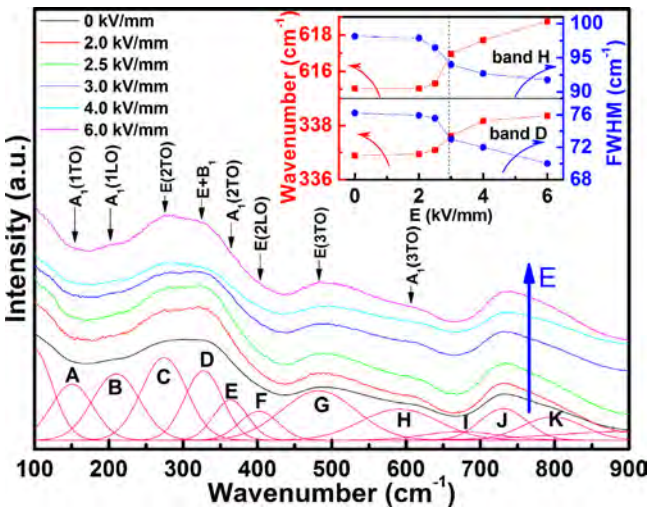

Fig. 10. Ex situ Raman spectra of the $x = 0.51$ sample poled under different electric fields. The inset shows the variation of the wavenumber and the FWHM for bands D and H as a function of poling field magnitude.

Fig. 10 indicates the ex situ Raman spectra recorded on the $x = 0.51$ sample poled under different electric fields at room temperature. All Raman peaks could be assigned to the well-known Raman active modes for typical ferroelectric perovskites (for example, PZT).[47] The diffuseness of Raman peaks means that there are obvious chemically ordered regions, in addition to both the short and long range polar order. No large difference between these Raman spectra could be detected, indicating that most of the changes caused by poling fields have been recovered after removal of electric fields. As a result, one can believe that the change of ergodic phases induced by external fields should be reversible. Nevertheless, some changes could still be found out if one looked into the details by deconvoluting all Raman peaks into different bands labeled as A to K from low to higher frequencies. The bands D and H, which correspond to the *A1*(2*TO*) and *A1*(3*TO*) modes from *B–O*(Ti(Mg)–O) bonds (200–400 cm^{-1}) and BO_6 (Ti(Mg)O_6) octahedra (400–900 cm^{-1})[48] respectively, were selected as examples to account for the variation of both the wavenumber and FWHM with electric fields, as indicated in the inset of Fig. 10. It can be seen that both the wavenumber and FWHMs for these two bands showed almost no changes as the poling field magnitude was lower than ~3 kV/mm. However, the FWHMs started to decrease and the corresponding Raman peaks tended to shift toward high frequencies after 3 kV/mm. The irreversible changes observed in the Raman spectra should be associated with the nonergodic phase initially existing in the $x = 0.51$ sample. These PNRs were aligned by external fields, resulting in a more ordered state.

Fig. 11 shows the in situ high-resolution synchrotron X-ray diffraction of the $x = 0.51$ sample under the application of different electric fields. Only $x = 0.51$ sample was analyzed here because it is representative of all studied samples. The (2 0 0) diffraction peak at zero field was found to be broad and asymmetric probably as a result of the diffuse scattering induced by the existence of PNRs.[49] The $x = 0.51$ sample might consist of a large number of PNRs with different sizes and symmetries as it is located at the boundary of ergodic and nonergodic states. In addition, no peak splitting of the (2 2 2) diffraction line further suggests that the average symmetry of the $x = 0.51$ sample should be initially pseudocubic. The same phenomenon was reported recently in BNT-based large-strain systems.[50–52] With increasing the electric field, the peak intensity of the (2 0 0) diffraction line increased while no obvious peak shift were observed till 2 kV/mm owing to the polarization alignment of PNRs under an external electric field.[53] However, it can be seen that the (2 2 2) diffraction pattern showed an obvious peak splitting, meaning that the average symmetry of the sample has transformed into a rhombohedral phase. This could be related to the transformation from an ergodic phase to a short-range ordered polar phase, thus leading to the first diffuse polarization current peak P_1 (Fig. 9) and the corresponding strain in this stage. This phase transition process is possible because the coexistence of ergodic phase and

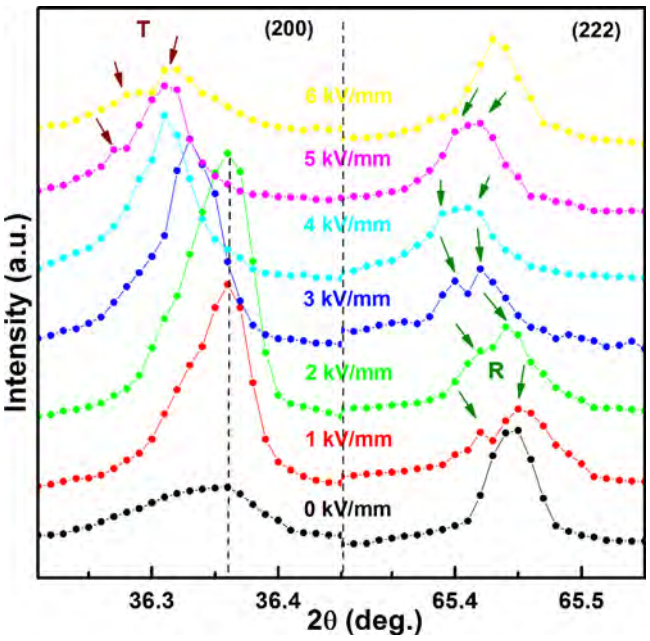

Fig. 11. Evolution of (2 0 0) and (2 2 2) diffraction lines for the $x = 0.51$ sample under different external electric fields.

nonergodic phase in the $x = 0.51$ composition means the minimum energy barrier. With further increasing the electric field ($3\,kV/mm \leq E \leq 5\,kV/mm$), one could observe an abrupt shift of the lower-angle side of the (2 0 0) and (2 2 2) peaks. However, no macroscopic symmetry change could be obviously detected. This means that the rhombohedral phase began to distort as the electric field was beyond the threshold field ($E > 3\,kV/mm$). Moreover, the (2 2 2) doublet tended to approach each other starting from 4 kV/mm, such that a weak tetragonal phase could be detected as $E \geq 5\,kV/mm$, as evidenced by the appearance of the low-angle shoulder of the (2 0 0) diffraction line. The characteristics of the long-range ferroelectric phase with a tetragonal symmetry became more distinct at $E = 6\,kV/mm$. The electric field induced phase structural transformation and the accompanying domain switching should be responsible for the second broad polarization current peak P_2 (Fig. 9). This should be possible in terms of their similar free energies because the $x = 0.51$ composition is very close to the MPB between PC and FE_T (Fig. 2). Therefore, the observed giant strain in the $x = 0.51$ sample could be ascribed to the accumulated effects of field-modulated reversible transformation from an ergodic relaxor to ferroelectric phase in which a crystallographic symmetry change is involved as well.

5. Conclusions

xBMT–$(0.75 - x)$PT–0.25BNT ($x = 0.35$–0.55) ternary ferroelectric ceramics were investigated in terms of their phase structure transition, dielectric behavior and ferroelectric polarization/strain characterizations. The substitution of BMT for PT was found to induce a ferroelectric pseudocubic–tetragonal morphotropic phase structural transition, accompanied by a relaxor–ferroelectric phase transformation in the studied composition range. This process was believed to be a result of the variation of the size and dynamics of the polar nanoregions, thus changing the domain morphology from nanodomains to macrodomains. Moreover, a coexistence of the ergodic phase and the nonergodic phase was found within a single pseudocubic phase zone for samples with $x = 0.50$ and 0.51 in the proximity of the morphotropic phase boundary ($0.47 < x < 0.50$). Surprisingly, an extremely large electromechanical strain up to 0.43% ($S_{max}/E_{max} = 621$ pm/V) was generated under a high bias field in the sample with $x = 0.51$. The generation of such a giant strain was ascribed to the accumulated effects of field-induced continuous and reversible phase transition from an ergodic phase to a complete polar phase, instead of a solely ferroelectric macrodomain switching.

Acknowledgements

The authors would like to thank Shanghai Synchrotron Radiation Source for use of the synchrotron radiation facilities. Financial support from the National Natural Science Foundation of China (Grant No. 51272060) and the Natural Science Foundation Anhui Province (Grant No. 1108085J14) is gratefully acknowledged.

References

1. Viehland D, Forst D, Xu Z, Li JF. lncommensurately modulated polar structures in antiferroelectric Sn-modified lead zirconate titanate: the modulated structure and its influences on electrically induced polarizations and strains. *J Am Ceram Soc* 1995;**78**:2101–12.
2. Park SE, Pan MJ, Markowski K, Yoshikawa S, Cross LE. Electric field induced phase transition of antiferroelectric lead lanthanum zirconate titanate stannate ceramics. *J Appl Phys* 1997;**82**:1798–803.
3. Brodeur RP, Gdchigi KW, Pruna PM, Shrout TR. Ultra-high strain ceramics with multiple field-induced phase transitions. *J Am Ceram Soc* 1994;**77**:3042–4.
4. Pan WY, Zhang QM, Bhalla A, Cross LE. Field-forced antiferroelectric-to-ferroelectric switching in modified lead zirconate titanate stannate ceramics. *J Am Ceram Soc* 1989;**72**:571–8.
5. Cross LE. Relaxor ferroelectrics: an overview. *Ferroelectrics* 1994;**151**:305–20.
6. Jang SJ, Uchino K, Nomura S, Cross LE. Electrostrictive behavior of lead magnesium niobate based ceramic dielectrics. *Ferroelectrics* 1980;**27**:31–4.
7. Uchino K, Nomura S, Cross LE, Jang SJ, Newnham RE. Electrostrictive effect in lead magnesium niobate single crystals. *J Appl Phys* 1980;**51**:1142–5.
8. Jaffe B, Cook WR, Jaffe H. *Piezoelectric ceramics*. London: Academic Press; 1971.
9. Kungl H, Theissmann R, Knapp M, Baehtz C, Fuess H, Wagner S, et al. Estimation of strain from piezoelectric effect and domain switching in morphotropic PZT by combined analysis of macroscopic strain measurements and synchrotron X-ray data. *Acta Mater* 2007;**55**:1849–61.
10. Li JY, Rogan RC, Üstündag E, Bhattacharya K. Domain switching in polycrystalline ferroelectric ceramics. *Nat Mater* 2005;**4**:776–81.
11. Zhang ST, Kounga AB, Aulbach E, Ehrenberg H, Rödel J. Giant strain in lead-free piezoceramics $Bi_{0.5}Na_{0.5}TiO_3$–$BaTiO_3$–$K_{0.5}Na_{0.5}NbO_3$ system. *Appl Phys Lett* 2007;**91**:112906.
12. Zuo RZ, Ye C, Fang XS, Li JW. Tantalum doped $0.94Bi_{0.5}Na_{0.5}TiO_3$–$0.06BaTiO_3$ piezoelectric ceramics. *J Eur Ceram Soc* 2008;**28**:871–7.
13. Jo W, Granzow T, Aulbach E, Rödel J, Damjanovic D. Origin of the large strain response in $(K_{0.5}Na_{0.5})NbO_3$-modified $(Bi_{0.5}Na_{0.5})TiO_3$–$BaTiO_3$ lead-free piezoceramics. *J Appl Phys* 2009;**105**:094102.

14. Pham KN, Hussain A, Ahn CW, Kim IW, Jeong SJ, Lee JS. Giant strain in Nb-doped $Bi_{0.5}(Na_{0.82}K_{0.18})_{0.5}TiO_3$ lead-free electromechanical ceramics. *Mater Lett* 2010;**64**:2219–22.
15. Wang FF, Xu M, Tang YX, Wang T, Shi WZ, Leung CM. Large strain response in the ternary $Bi_{0.5}Na_{0.5}TiO_3$–$BaTiO_3$–$SrTiO_3$ solid solutions. *J Am Ceram Soc* 2012;**95**:1955–9.
16. Dul'kin E, Mojaev E, Roth M, Jo W, Granzow T. Acoustic emission study of domain wall motion and phase transition in $(1-x-y)Bi_{0.5}Na_{0.5}TiO_3$–$xBaTiO_3$–$yK_{0.5}Na_{0.5}NbO_3$ lead-free piezoceramics. *Scr Mater* 2009;**60**:251–3.
17. Jo W, Schaab S, Sapper E, Schmitt LA, Kleebe HJ, Bell AJ, et al. On the phase identity and its thermal evolution of lead free $(Bi_{1/2}Na_{1/2})TiO_3$–6 mol% $BaTiO_3$. *J Appl Phys* 2011;**110**:074106.
18. Daniels JE, Jo W, Rödel J, Rytz D, Donner W. Structural origins of relaxor behavior in a $0.96(Bi_{1/2}Na_{1/2})TiO_3$–$0.04BaTiO_3$ single crystal under electric field. *Appl Phys Lett* 2011;**98**:252904.
19. Kling J, Jo W, Dittmer R, Schaab S, Kleebe HJ. Temperature-dependent phase transitions in the lead-free piezoceramics $(1-x-y)(Bi_{1/2}Na_{1/2})TiO_3$–$xBaTiO_3$–$y(K_{0.5}Na_{0.5})NbO_3$ observed by in situ transmission electron microscopy and dielectric measurements. *J Am Ceram Soc* 2013;**96**:3312–24.
20. Jo W, Daniels J, Damjanovic D, Kleemann W, Rödel J. Two-stage processes of electrically induced-ferroelectric to relaxor transition in $0.94(Bi_{1/2}Na_{1/2})TiO_3$–$0.06BaTiO_3$. *Appl Phys Lett* 2013;**102**:192903.
21. Fan LL, Chen J, Kang HJ, Liu LJ, Fang L, Deng JX, et al. Structure, piezoelectric, and ferroelectric properties of $BaZrO_3$ substituted $Bi(Mg_{1/2}Ti_{1/2})O_3$–$PbTiO_3$ perovskite. *J Appl Phys* 2012;**111**:104118.
22. Chen J, Li JY, Fan LL, Zou N, Ji PF, Liu LJ, et al. Enhanced piezoelectric and antiferroelectric properties of high-T_c perovskite of Zr-substituted $Bi(Mg_{1/2}Ti_{1/2})O_3$–$PbTiO_3$. *J Appl Phys* 2012;**112**:074101.
23. Khalyavin DD, Salak AN, Vyshatko NP, Lopes AB, Olekhnovich NM, Pushkarev AV, et al. Crystal structure of metastable perovskite $Bi(Mg_{1/2}Ti_{1/2})O_3$: Bi-based structural analogue of antiferroelectric $PbZrO_3$. *Chem Mater* 2006;**18**:5104–10.
24. Dai XH, Xu Z, Li JF, Viehland D. Field-induced strains and polarization switching mechanisms in La-modified lead zirconate titanate ceramics. *J Appl Phys* 1996;**79**:2023–8.
25. Hoffmann MJ, Hammer M, Endriss A, Lupascu DC. Correlation between microstructure, strain behavior, and acoustic emission of soft PZT ceramics. *Acta Mater* 2001;**49**:1301–10.
26. Fu J, Zuo RZ. Giant electrostrains accompanying the evolution of a relaxor behavior in $Bi(Mg,Ti)O_3$–$PbZrO_3$–$PbTiO_3$ ferroelectric ceramics. *Acta Mater* 2013;**61**:3687–94.
27. Choi SY, Jeong SJ, Lee DS, Kim MS, Lee JS, Cho JH, et al. Gigantic electrostrain in duplex structured alkaline niobates. *Chem Mater* 2012;**24**:3363–9.
28. Damjanovic D. A morphotropic phase boundary system based on polarization rotation and polarization extension. *Appl Phys Lett* 2010;**97**:062906.
29. Suchomel MR, Daviesa PK. Enhanced tetragonality in $(x)PbTiO_3$–$(1-x)Bi(Zn_{1/2}Ti_{1/2})O_3$ and related solid solution systems. *Appl Phys Lett* 2005;**86**:262905.
30. Shimojo Y, Wang R, Sekiya T, Nakamura T, Cross LE. MPB phase diagram and ferroelectric properties in the $PbTiO_3$–$BiScO_3$ system. *Ferroelectrics* 2003;**284**:121–8.
31. Randall CA, Eitel R, Jones B, Shrout TR, Woodward DI, Reaney IM. Investigation of a high T_c piezoelectric system: $(1-x)Bi(Mg_{1/2}Ti_{1/2})O$–$(x)PbTiO_3$. *J Appl Phys* 2004;**95**:3633–9.
32. Kuharuangrong S, Schulze W. Characterization of $Bi_{0.5}Na_{0.5}TiO_3$–$PbTiO_3$ dielectric materials. *J Am Ceram Soc* 1996;**79**:1273–80.
33. Chen A, Jing Z, Yu Z. Ferroelectric relaxor $Ba(Ti,Ce)O_3$. *J Phys: Condens Matter* 2002;**14**:8901–12.
34. Uchino K, Nomura S. Critical exponents of the dielectric constants in diffused-phase-transition crystals. *Ferroelectr Lett* 1982;**44**:55–61.
35. Chen W, Yao X, Wei XY. Tunability and ferroelectric relaxor properties of bismuth strontium titanate ceramics. *Appl Phys Lett* 2007;**90**:182902.
36. Novak N, Pirc R, Wencka M, Kutnjak Z. High-resolution calorimetric study of $Pb(Mg_{1/3}Nb_{2/3})O_3$ single crystal. *Phys Rev Lett* 2012;**109**:037601.
37. Cross LE. Relaxor ferroeolectrics. *Ferroelectrics* 1987;**76**:241–67.
38. Viehland D, Jang SJ, Cross LE, Wuttig M. Freezing of the polarization fluctuations in lead magnesium niobate relaxors. *J Appl Phys* 1990;**68**:2916–21.
39. Burns G, Dacol FH. Crystalline ferroelectrics with glassy polarization behavior. *Phys Rev B* 1983;**28**:2527–30.
40. Samara GA. The relaxational properties of compositionally disordered ABO_3 perovskites. *J Phys: Condens Matter* 2003;**15**:R367–411.
41. Xie L, Li YL, Yu R, Cheng ZY, Wei XY, Yao X, et al. Static and dynamic polar nanoregions in relaxor ferroelectric $Ba(Ti_{1-x}Sn_x)O_3$ system at high temperature. *Phys Rev B* 2012;**85**:014118.
42. Dai XH, DiGiovanni A, Viehland D. Dielectric properties of tetragonal lanthanum modified lead zirconate titanate ceramics. *J Appl Phys* 1993;**74**:3399–405.
43. Bokov AA, Ye ZG. Recent progress in relaxor ferroelectrics with perovskite structure. *J Mater Sci* 2006;**41**:31–52.
44. Viola G, Ning HP, Wei XJ, Deluca M, Adomkevicius A, Khaliq J, et al. Dielectric relaxation, lattice dynamics and polarization mechanisms in $Bi_{0.5}Na_{0.5}TiO_3$-based lead-free ceramics. *J Appl Phys* 2013;**114**:014107.
45. Shieh J, Wu KC, Chen CS. Switching characteristics of MPB compositions of $(Bi_{0.5}Na_{0.5})TiO_3$–$BaTiO_3$–$(Bi_{0.5}K_{0.5})TiO_3$ lead-free ferroelectric ceramics. *Acta Mater* 2007;**55**:3081–7.
46. Pirc R, Blinc R. Vogel–Fulcher freezing in relaxor ferroelectrics. *Phys Rev B* 2007;**76**:020101.
47. Lima KCV, Filho AGS, Ayala AP, Filho JM, Freire PTC, Melo FEA, et al. Raman study of morphotropic phase boundary in $PbZr_{1-x}Ti_xO_3$ at low temperatures. *Phys Rev B* 2001;**63**:184105.
48. Schütz D, Deluca M, Krauss W, Feteira A, Jackson T, Reichmann K. Lone-pair-induced covalency as the cause of temperature- and field-induced instabilities in bismuth sodium titanate. *Adv Funct Mater* 2012;**22**:2285–94.
49. Perrin C, Menguy N, Suard E, Muller Ch, Caranoni C, Stepanov A. Neutron diffraction study of the relaxor-ferroelectric phase transition in disordered $Pb(Sc_{1/2}Nb_{1/2})O_3$. *J Phys: Condens Matter* 2000;**12**:7523–39.
50. Daniels JE, Jo W, Rödel J, Jones JL. Electric-field-induced phase transformation at a lead-free morphotropic phase boundary: case study in a $93\%(Bi_{0.5}Na_{0.5})TiO_3$–$7\%BaTiO_3$ piezoelectric ceramic. *Appl Phys Lett* 2009;**95**:032904.
51. Daniels JE, Jo W, Rödel J, Honkimöki V, Jones JL. Electric-field-induced phase-change behavior in $(Bi_{0.5}Na_{0.5})TiO_3$–$BaTiO_3$–$(K_{0.5}Na_{0.5})NbO_3$: a combinatorial investigation. *Acta Mater* 2010;**58**:2103–11.
52. Simons H, Daniels JE, Jo W, Dittmer R, Studer A, Avdeev M, et al. Electric-field-induced strain mechanisms in lead-free $94\%(Bi_{1/2}Na_{1/2})TiO_3$–$6\%BaTiO_3$. *Appl Phys Lett* 2011;**98**:082901.
53. Guo HZ, Ma C, Liu XM, Tan XL. Electrical poling below coercive field for large piezoelectricity. *Appl Phys Lett* 2013;**102**:092902.